AN EXPERIMENTAL REALISATION OF STEADY SPANWISE FORCING FOR TURBULENT DRAG REDUCTION

***M.W. Knoop*[1], *F.H. Hartog*[1,2], *F.F.J. Schrijer*[1], *and B.W. van Oudheusden*[1]**

[1]**Aerodynamics Group, Faculty of Aerospace Engineering, Delft University of Technology**
[2]**Dimple Aerospace B.V.**

m.w.knoop@tudelft.nl

July 21, 2023

Abstract

This work presents an experimental realization of steady spatial spanwise forcing of a turbulent boundary layer, with the aim of turbulent drag reduction (DR). Actuation is performed with a setup, consisting of a streamwise oriented array of four spanwise running belts, that run in alternating direction, so as to generate a spatial square-wave. The receptivity of the turbulent boundary layer to the forcing is investigated using stereoscopic particle image velocimetry, for a waveform of $\lambda_x^+ = 400$ at various amplitudes. A significant control effect is realized. The DR increases monotonically with amplitude, which is in qualitative agreement with the available literature. A maximum DR of 25% is observed. In view of the limited spatial extent of the actuation surface, the DR is expected to increase even further as a result of its streamwise transient. The second-order turbulence statistics reveal an attenuation up to $y^+ \approx 100$, the magnitude of this effect is correlated to the amplitude. Specifically, a maximum streamwise stress reduction of 44% is found, and the integral turbulence kinetic energy production is reduced by 39%. The scalar fields of the streamwise stress reveal that the stress attenuation shows a shorter spatial transient compared to the expected transient of the DR.

1 Introduction

Turbulent drag reduction is a crucial research area in fluid dynamics, as reducing drag can lead to substantial energy savings and emission reductions in a variety of industrial and transportation applications. In this work we focus on spanwise forcing through wall motion, involving a spatio-temporal, in-plane, wall oscillation in the spanwise direction. The energy expenditure associated with the wall forcing is related to the theoretical power input necessary to drive the spanwise profile. Subsequently, the net power saving (NPS) is the difference between DR and this energy input.

Both temporal and spatio-temporal forcing, referred to as oscillating wall (OW) and travelling wave (TW) forcing, have been extensively researched, in both numerical and experimental studies. DR values of over 40% have been reported (Ricco et al., 2021). Despite its high DR and NPS potential, purely spatial forcing, also referred to as standing wave (SW) forcing, has seen less attention with only a small number of numerical papers investigating this strategy (e.g. Skote, 2013; Viotti et al., 2009; Yakeno et al., 2009). Viotti et al., 2009 showed that compared to OW forcing, the DR margin for SW forcing is about 20-30% higher, for similar actuation parameters under a convective transformation. SW forcing imposes a wall velocity in the form of:

$$W_w(x) = A \sin\left(\frac{2\pi}{\lambda_x} x\right), \tag{1}$$

where A is the spanwise velocity amplitude and λ_x is the streamwise wavelength of actuation. In this paper, the streamwise, wall-normal, and spanwise coordinates are denoted by x, y, and z, respectively, which correspond to the instantaneous velocities u, v, and w. Reynolds decomposition into the mean and fluctuation component is applied, indicated by an overbar and prime, respectively. Viscous scaling is performed with the kinematic viscosity ν and the friction velocity $u_\tau \equiv \sqrt{\tau_w/\rho}$; τ_w and ρ are the wall shear stress and fluid density, respectively. Scaling is applied using either a reference $u_{\tau 0}$ of the non-actuated case or the actual friction velocity u_τ, indicated by the superscripts '$+$' and '$*$', respectively. Regarding the performance of SW forcing, an optimum DR had been reported around $\lambda_x^+ = 1000 - 1250$. The DR shows a monotonic increase, at a decreasing rate, as a function of A^+, for a maximum DR of 52% at $A^+ = 20$ (Viotti et al., 2009).

The mechanism responsible for the DR lies in part in the oscillatory nature of the resulting spanwise velocity profile. Ricco (2004) presented evidence that this breaks up the interaction between the near-wall streaks and the quasi-streamwise vortices by laterally displacing the two features. Their disrupted spatial coherence decreases the strength of the near-wall cycle

resulting in a drag-reduced state.

In order to address the sparse attention devoted towards SW forcing, especially in experimental setting, this work presents a novel concept for implementing spatial spanwise forcing in external flows. The concept was inspired by the experiment of Kiesow and Plesniak (2003), who employed a single spanwise running belt to study the response of the turbulent boundary layer to a steady spanwise crossflow. Extending their idea, the turbulent boundary layer can be forced by a series of belts running in alternating spanwise directions, to create a SW like forcing. As a proof of concept, an experimental setup was realized which consisted of four spanwise running belts. The aim of this apparatus was to assess the effectiveness of flow control and to characterize the aerodynamic response. The results elaborate on the mean velocity profiles, DR characteristics, and higher-order turbulence statistics. Lastly, we present a discussion on the spatial transient of streamwise Reynolds stress over the actuation surface.

2 Methodology

The experimental setup is referred to as the steady spanwise excitation setup (SSES). A schematic representation of the SSES is presented in Figure 1. The setup consists of an array of four streamwise-spaced, spanwise-running belts, which run in alternating direction, thereby creating a spatial square-wave boundary condition. The use of square-waves is justified by the studies of Cimarelli et al. (2013) and Mishra and Skote (2015), who showed substantial DR and NPS values can be achieved for non-sinusoidal forcing. Four neoprene belts with a belt width of 9 mm are used, covering a spanwise distance of 256 mm. A small streamwise separation, of 2 mm, between the belts is required in order to realize the design mechanically. This resulted in a sequence of two waveforms with a wavelength of $\lambda_x^+ = 22$ mm. We define the start of the waveform, and the origin of the coordinate system, at 1 mm (i.e. half the streamwise separation) upstream of the first belt. To ensure a seamless alignment with the wall, the belts are integrated into an aluminium surface plate. Precise tolerances are set for the grooves to minimize any gaps, with a strict limit of 50 µm for both maximum gap and step size. To power the belts, a non-slip pulley system is employed, driven by two AC servo motors that run in the positive and negative spanwise direction. The setup is designed to run from 0-2,000 RPM corresponding to a maximum spanwise velocity of 6 m/s. An advantage of the current experimental setup is the independent control over the actuation parameters, A^+ and λ_x^+, whereas the amplitude and period are coupled in OW and TW forcing that is realized using oscillatory elements at a fixed displacement amplitude. A^+ is directly controlled by setting the belt speed, and λ_x^+ can be changed by altering the viscous scaling parameter.

Wind tunnel experiments were conducted in the M-tunnel at the Delft University of Technology. The open return tunnel has a square test section of 0.4 m × 0.4 m. Measurements were made at a freestream velocity of $U_\infty = 6.7$ m/s, at a freestream turbulence intensity of approximately 0.7%. A clean turbulent boundary layer was generated using a plate with an elliptical leading edge and tripped using carborundum roughness (24 grit), achieving a development length of 3 m. The boundary layer thickness (δ), and subsequently the friction Reynolds number ($Re_\tau \equiv \delta u_{\tau 0}/\nu$), were obtained from hot-wire anemometer measurements of the non-actuated boundary layer. For the current experiments the conditions are $\delta = 67.4$ mm, $u_{\tau 0} = 0.27$ m/s and $Re_\tau = 1230$. The experimental apparatus was placed downstream of the wind tunnel exit, in an open-jet configuration. A schematic representation of the experimental setup is depicted in Figure 2.

Stereoscopic particle image velocimetry (PIV) was performed to measure the three velocity components in the $x - y$ plane. Each measurement consists of 1000 uncorrelated velocity fields, acquired at a frequency of 10 Hz. Two fields of view (FOVs) are considered. To obtain ensemble averaged turbulence statistics at high spatial resolution, FOV1 was used, centred over the central two belts, spanning 24 mm × 14.5 mm in the streamwise and wall-normal direction, respectively. FOV2 was used to assess the spatial development of turbulence statistics, covering the four belts, for a size of 46.5 mm × 17.5 mm. Imaging was achieved with two LaVision sCMOS cameras (2560 × 2160 pixels), fitted with Nikkor AF-S 200mm lenses, and a f/11 aperture. For FOV1, additional 2× teleconverters were used, for an effective focal length of 400mm. The cameras were oriented at $\pm 30^\circ$ with respect to the laser sheet normal, and Scheimpflug adapters were used for uniform focus. Illumination was provided by a Quantel Evergreen 200 laser, generating a laser sheet of approximately 1 mm thickness. Seeding was provided by a fog machine to create 1 µm tracer particles from a water-glycol mixture.

Stereo-calibration, self-calibration and vector calculations were performed in LaVision DaVis10.2. The individual two-component velocity fields were obtained using cross-correlation, with circular 16 × 16 pixels interrogation windows at 75% overlap. The final vector spacings were 0.035 mm ($0.64\nu/u_{\tau 0}$) and 0.067 mm ($1.2\nu/u_{\tau 0}$) for FOV1 and FOV2, respectively. The resultant fields were combined using a least squares fitting approach to obtain 2D3C velocity fields. The turbulence statistics were ensemble averaged (indicated by $\langle\rangle$) over time and streamwise direction, spanning $0.5 \leq x/\lambda_x \leq 1.5$. This choice was made to assess the integral effect of actuation over one streamwise phase. The uncertainties at $y^+ = 15$ of the ensemble averaged turbulence statistics, from the uncorrelated samples (i.e. every fourth streamwise vector), are 0.069% and 0.36% for the mean streamwise

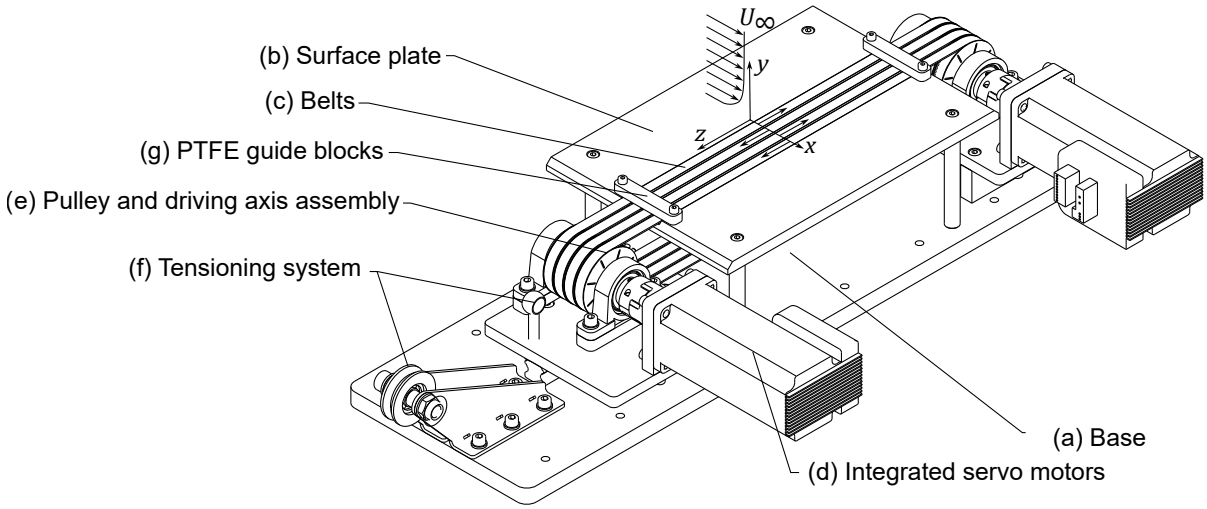

Figure 1: Schematic of the SSES mechanism

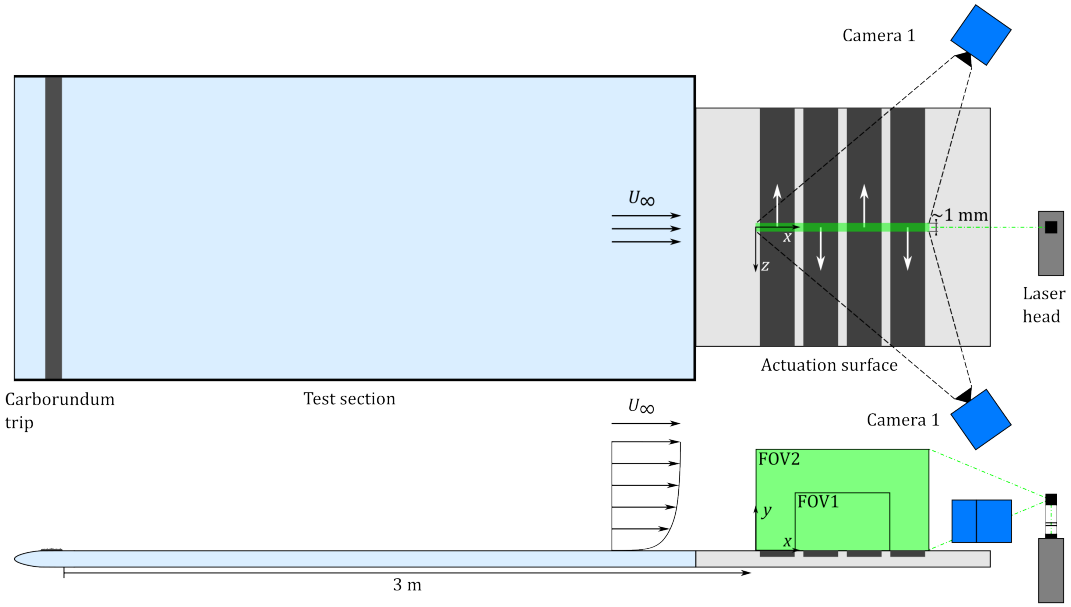

Figure 2: Schematic representation of the experimental setup

velocity and streamwise Reynolds stress, respectively.

The reference friction velocity was obtained from a fit to the inner-layer profile of Chauhan et al. (2009). To constrain the fitting procedure in order to obtain consistent values, the log-layer parameters are kept constant, where standard values of $\kappa = 0.384$ and $B = 4.17$ have been used (Nagib & Chauhan, 2008). As the actuated cases deviate from the canonical behaviour, u_τ was instead estimated by fitting the region $3 \leq y^+ \leq 5.5$ to the linear sublayer profile $u^* = y^*$. The region of interest encompassed a set of four data points. Following this DR is calculated as $\mathrm{DR} = 1 - \tau_w/\tau_{w0}$. From all considered cases, the maximum mean absolute percentage error of the fit was 2.7%.

3 Results and discussion

The freestream conditions were selected such that $\lambda_x^+ = 400$, while six spanwise velocity amplitudes were investigated, ranging from $A^+ \approx 2 - 12$. We present the results for the DR and ensemble averaged turbulence statistics profiles obtained from FOV1. Subsequently, we discuss the spatial distribution of streamwise normal stress obtained from FOV2.

Mean velocity and drag characteristics

The mean streamwise velocity profiles are depicted in Figure 3(a,b), in scaling with the reference and actual friction velocity, respectively. Scaling with $u_{\tau 0}$ shows a decrease in mean velocity in the region $y^+ \leq 15$, indicative of a drag-reduced flow state and in line with previous studies (Jung et al., 1992; Ricco et al., 2021; Ricco & Wu, 2004). This is further emphasised when scaling with u_τ. The profiles show similarity

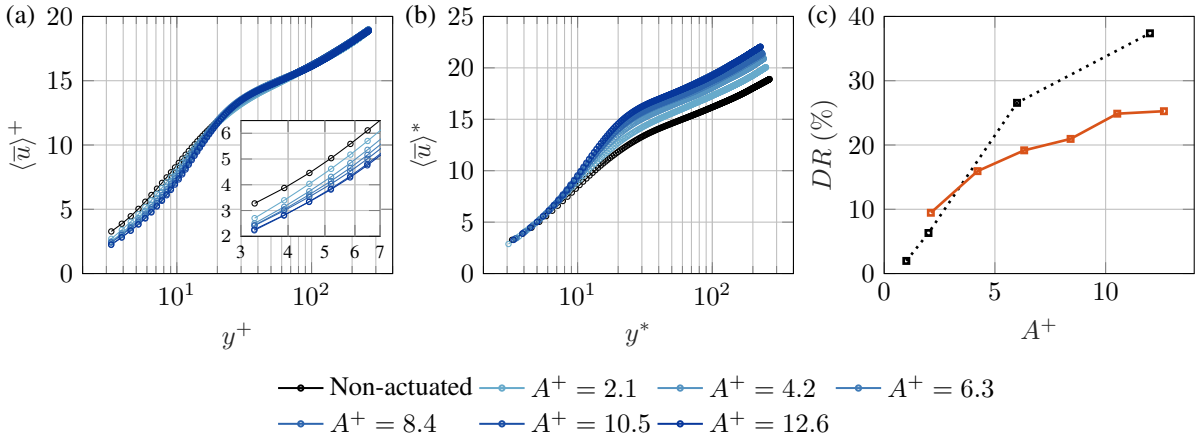

Figure 3: (a-b) Streamwise velocity profiles for the non-actuated case and cases with $\lambda_x^+ = 400$, (a) scaling with $u_{\tau 0}$, (b) scaling with u_τ. (c) DR vs A^+ (solid) compared to the DNS results of Viotti et al., 2009 for $\lambda_x^+ = 300$ (dotted).

in the viscous sublayer but with an upward shift of the logarithmic region under actuation, consistent with the reduction in skin friction (Gatti & Quadrio, 2016).

The DR characteristics as a function of A^+ are presented in FIG. 3(c), where the DNS results of Viotti et al., 2009, subject to Equation 1 at $\lambda_x^+ = 300$ and $Re_\tau = 200$, are added for reference. In line with the behaviour of the mean velocity profiles, the DR in the experiments increases with A^+, reaching a maximum value of 25%. Qualitatively the trends of literature are matched but at a lower magnitude for higher values of A^+. This is primarily attributed to the fact that the measurement region is likely still within the rising spatial transient of DR. Ricco and Wu, 2004 show that the DR exhibits a steep increase over a streamwise extent of approximately 3δ, from the onset of actuation, settling on a maximum steady value, whereas FOV1 only extends over $0.16 \leq x/\delta \leq 0.50$. Secondly, as shown by Gatti and Quadrio (2016), a slight reduction in performance is expected due to the higher friction Reynolds number in the current experiments compared to the DNS study. Moreover, the experimental realization may not perform to the same degree as the idealized conditions in the numerical studies, due to step changes in surface roughness (belts) and small surface gaps associated with the tolerances.

Higer-order turbulence statistics

The streamwise and spanwise turbulent stresses as well as the premultiplied turbulence kinetic energy (TKE) production are presented in FIG. 4. Scaling is performed with $u_{\tau 0}$ to highlight the absolute changes with respect to the non-actuated case. Assessing the streamwise stress $\langle u'^2 \rangle^+$, we can observe that actuation attenuates the energy in the region up to $y^+ \approx 100$. In line with the previously observed trend in DR, the reduction in stress increases at a decreasing rate with A^+. The near-wall peak is significantly reduced and shifted to higher wall-normal locations, with a maximum peak reduction of 44%. In the spanwise stress component $\langle w'^2 \rangle^+$, a strong peak is observed in the near-wall region (note the log-log scale). This peak is a direct result from the phase-wise averaged component of the spanwise stress, corresponding to the variance of the spanwise velocity profile. Therefore the peak's magnitude is correlated to the spanwise velocity amplitude. The peak decays in magnitude when moving in the wall-normal direction. Furthermore, the wall-normal penetration of this peak increases with A^+. Lastly, we assess the production of TKE. Similarly to the streamwise stress, the production is significantly attenuated up to a region of $y^+ \approx 100$, and the near-wall peak is shifted to higher wall-normal locations. A maximum reduction in TKE production of 39% is found for the considered wall-normal region.

Spatial transient of streamwise normal stress

We have shown that a significant flow control effect can be achieved with the proposed experimental setup. Specifically, the streamwise normal stress shows a strong reduction of the near-wall peak intensity. Therefore we elaborate on the spatial distribution of the streamwise normal stress. Figure 5(a,b) depicts the scalar-fields of $\langle u'^2 \rangle^+$ for the non-actuated case and actuation at $A^+ = 12.6$, respectively. The streamwise coordinate is scaled shown with both the streamwise wavelength of actuation (λ_x) and boundary layer thickness (δ). This investigation serves two purposes: firstly, to study the spatial response of the streamwise normal stress under actuation; and secondly, to assess the validity of space-averaging the various turbulence statistics in the streamwise direction.

The scalar field for the non-actuated case shows a clear energetic peak at the characteristic location $y^+ = 15$. Albeit for some slight variance, the energy peak stays constant in magnitude, location, and peak width, over the streamwise extent. When actuation is performed, the stress is not significantly affected upstream of the actuation surface. Moving in the stream-

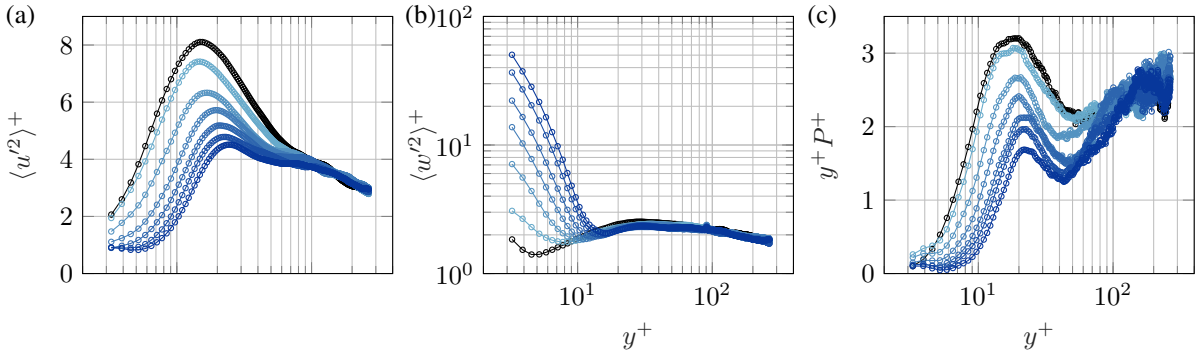

Figure 4: (a) Streamwise Reynolds stress, (b) spanwise Reynolds stress, plotted on a log-log scale and (c) premultiplied production or turbulence kinetic energy. The production term is approximated by $P = -\langle u'v'\rangle \mathrm{d}\langle\overline{u}\rangle/\mathrm{d}y$ (Panton, 2001), in premultiplied form, an equal area highlights an equal contribution to the TKE production. Legend depicted in Figure 3

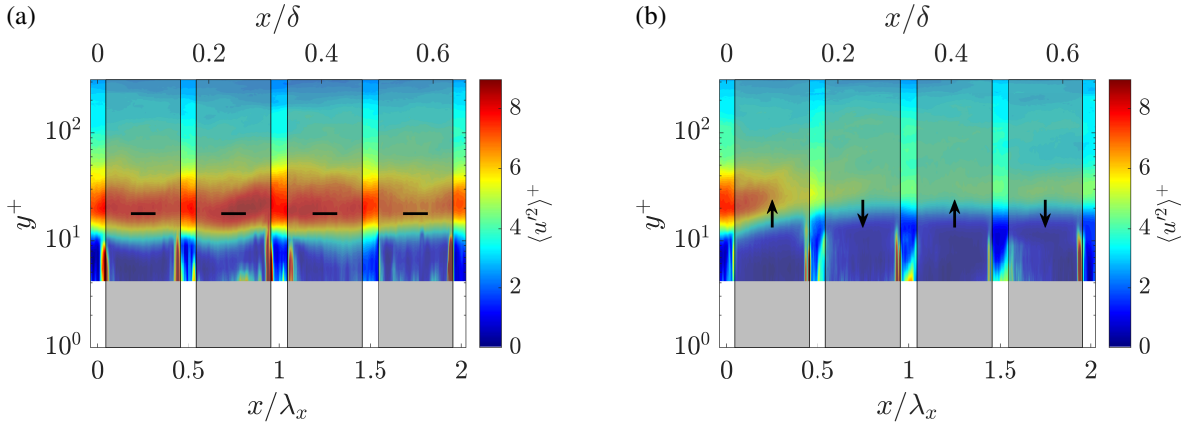

Figure 5: Scalar fields of streamwise Reynolds stress ($\langle u'^2\rangle^+$) for (a) non-actuated case and (b) actuation at $A^+ = 12.6$. The grey shaded areas and corresponding arrows indicate the regions over the belts, and their respective rotation direction.

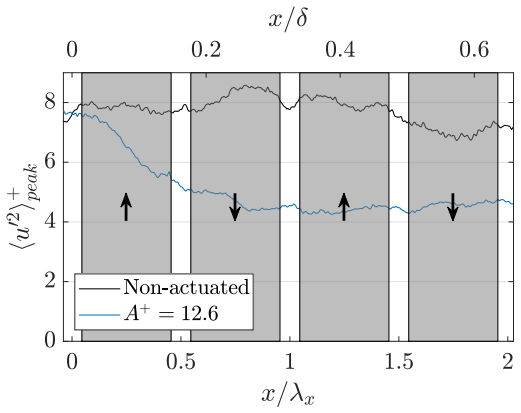

Figure 6: Spatial development of the magnitude of the streamwise Reynolds stress peak for the two cases as considered in Figure 5.

wise direction, a strong reduction of the near-wall stress peak is observed over the first belt, followed by a more gradual transition to an equilibrium energy state from $x/\lambda_x \approx 0.75$, or $x/\delta \approx 0.22$, onward. To further quantify the effect, Figure 6 depicts the spatial distribution of the streamwise stress peak, for the actuated and non-actuated case. An interesting conclusion from this analysis is that the spatial transient of the streamwise stress appears to be much smaller compared to that of the DR. As aforementioned, the DR shows a spatial transient in the region $x/\delta \leq 3$, in contrast to $x/\delta \leq 0.22$ for the streamwise stress. This suggests that the DR lags behind and requires a longer development length to establish compared to the energy attenuation.

Assessing both the scalar fields, specifically in the region $y^+ \leq 10$, strong local energy peaks can be observed in the leading- and trailing edge regions of the belts. We believe these are non-physical stress peaks, resulting from unsteady reflections on the spanwise surface grooves of the aluminium plate that the belts run in. Referring back to the integral streamwise stress over the central two belts (i.e. FOV1) in Figure 4 (a), it can be observed that these spurious stresses do not significantly increase the near-wall energy. Even though a small transient over the second belt can be observed, streamwise averaging the scalar fields in FOV1, span-

ning $0.5 \leq x/\lambda_x \leq 1.5$, is believed to be a valid choice to assess the integral effect of actuation over one wavelength of actuation in the current experiment.

4 Concluding remarks

Despite its DR and NPS potential, SW forcing has seen relatively little attention in the literature, in comparison to OW an TW forcing. A small number of numerical studies investigate spatial forcing, while no experimental work focuses on SW specifically. To bridge this gap, we proposed a concept, employing a series of spanwise running belts, to realize the steady spatial forcing in external boundary layer flows. The experimental setup consisted of four belts, rotating in alternating spanwise direction. An advantage of a setup like this, compared to OW or TW forcing with oscillatory elements at a fixed displacement amplitude, is the independent control over A^+ and λ_x^+.

The experimental setup was found to be effective in realising a significant flow control effect for turbulent DR. A reduction of mean streamwise velocity in the region $y^+ \leq 15$ was observed, indicative of a drag-reduced flow state. The reduction was positively correlated to the spanwise velocity amplitude. From the velocity profiles a maximum DR value of 25% was found. The DR is expected to increase further as a result of its spatial transient. Accordingly, the turbulent fluctuations were strongly attenuated, with a maximum peak streamwise stress reduction of 44%. Furthermore, we observe a drop in TKE production of 39%. The spatial transient of streamwise Reynolds stress revealed a steep drop in energy over the first belt, followed by reduction to an approximately steady-state energy reduction at around $x/\delta \approx 0.22$. An interesting finding is that the transient of the streamwise stress extends over a much smaller spatial extent compared to the DR, which shows a transient over the spatial extent of 3δ (Ricco & Wu, 2004).

These results motivate further research, exploring the flow mechanisms and the response to the governing actuation parameters. Recommendations for a future experimental setup are a longer streamwise extent of the actuation surface to investigate the spatial transient as well as the steady-state DR response. Furthermore, the belt width can be increased to achieve actuation wavelengths in the order of the optimum found in the literature.

Acknowledgments

This work was financially supported by the Netherlands Enterprise Agency under grant number TSH21002. The authors convey their sincere appreciation to Ir. Michiel van Nesselrooij and Ir. Drs. Olaf van Campenhout from Dimple Aerospace B.V. for their support in realizing the experimental setup and for the acquisition of the grant. The authors wish to give special thanks to BerkelaarMRT B.V. for the mechanical design and realisation of the experimental apparatus.

References

Chauhan, K. A., Monkewitz, P. A., & Nagib, H. M. (2009). Criteria for assessing experiments in zero pressure gradient boundary layers. *Fluid Dynamics Research*, *41*(2), 021404.

Cimarelli, A., Frohnapfel, B., Hasegawa, Y., De Angelis, E., & Quadrio, M. (2013). Prediction of turbulence control for arbitrary periodic spanwise wall movement. *Physics of Fluids*, *25*(7), 075102.

Gatti, D., & Quadrio, M. (2016). Reynolds-number dependence of turbulent skin-friction drag reduction induced by spanwise forcing. *Journal of Fluid Mechanics*, *802*, 553–582.

Jung, W. J., Mangiavacchi, N., & Akhavan, R. (1992). Suppression of turbulence in wall-bounded flows by high-frequency spanwise oscillations. *Physics of Fluids A: Fluid Dynamics*, *4*(8), 1605–1607.

Kiesow, R. O., & Plesniak, M. W. (2003). Near-wall physics of a shear-driven three-dimensional turbulent boundary layer with varying cross-flow. *Journal of Fluid Mechanics*, *484*, 1–39.

Mishra, M., & Skote, M. (2015). Drag reduction in turbulent boundary layers with half wave wall oscillations. *Mathematical Problems in Engineering*, *2015*.

Nagib, H. M., & Chauhan, K. A. (2008). Variations of von kármán coefficient in canonical flows. *Physics of Fluids*, *20*(10), 101518.

Panton, R. L. (2001). Overview of the self-sustaining mechanisms of wall turbulence. *Progress in Aerospace Sciences*, *37*(4), 341–383.

Ricco, P. (2004). Modification of near-wall turbulence due to spanwise wall oscillations. *Journal of Turbulence*, *5*(1), 024.

Ricco, P., Skote, M., & Leschziner, M. A. (2021). A review of turbulent skin-friction drag reduction by near-wall transverse forcing. *Progress in Aerospace Sciences*, *123*, 100713.

Ricco, P., & Wu, S. (2004). On the effects of lateral wall oscillations on a turbulent boundary layer. *Experimental Thermal and Fluid Science*, *29*(1), 41–52.

Skote, M. (2013). Comparison between spatial and temporal wall oscillations in turbulent boundary layer flows. *Journal of Fluid Mechanics*, *730*, 273–294.

Viotti, C., Quadrio, M., & Luchini, P. (2009). Streamwise oscillation of spanwise velocity at the wall of a channel for turbulent drag reduction. *Physics of Fluids*, *21*.

Yakeno, A., Hasegawa, Y., & Kasagi, N. (2009). Spatio-temporally periodic control for turbulent friction drag reduction. *Sixth International Symposium on Turbulence and Shear Flow Phenomena*.